ISSN 1674-1056
http://cpb.iphy.ac.cn
http://iopscience.iop.org/cpb
中国物理 B
Chinese Physics
中国物理 Chinese Physics B

Basic features of the multiscale interaction between tearing modes and slab ion-temperature-gradient modes

L Wei(魏来)[1], Z X Wang(王正汹)[1], J Q Li(李继全)[2], Z Q Hu(胡朝清)[1], Y Kishimoto(岸本泰明)[3]
Citation: Chin. Phys. B . 2019, 28(12): 125203 . **doi:** 10.1088/1674-1056/ab5437
Journal homepage: http://cpb.iphy.ac.cn; http://iopscience.iop.org/cpb

What follows is a list of articles you may be interested in

Formation of electron depletion layer and parallel electric field in the separatrix region of anti-parallel magnetic reconnection

Zisheng Li(李子圣), Huanyu Wang(王焕宇), Xinliang Gao(高新亮)
Chin. Phys. B . 2019, 28(7): 075203 . **doi:** 10.1088/1674-1056/28/7/075203

Preliminary investigation on electrothermal instabilities in early phases of cylindrical foil implosions on primary test stand facility

Guanqiong Wang(王冠琼), Delong Xiao(肖德龙), Jiakun Dan(但家坤), Yang Zhang(张扬), Ning Ding(丁宁), Xianbin Huang(黄显宾), Xiaoguang Wang(王小光), Shunkai Sun(孙顺凯), Chuang Xue(薛创), Xiaojian Shu(束小建)
Chin. Phys. B . 2019, 28(2): 025203 . **doi:** 10.1088/1674-1056/28/2/025203

Numerical analysis of the optimized performance of the electron cyclotron wave system in a HL-2M tokamak

Jing-Chun Li(李景春), Xue-Yu Gong(龚学余), Jia-Qi Dong(董家齐), Jun Wang(王俊), Lan Yin(尹岚)
Chin. Phys. B . 2016, 25(4): 045201 . **doi:** 10.1088/1674-1056/25/4/045201

Effects of *q*-profiles of a weak magnetic shear on energetic ion excited *q*=1 mode in tokamak plasmas

Ze-Yu Li(李泽宇), Xian-Qu Wang(王先驱), Xiao-Gang Wang(王晓钢)
Chin. Phys. B . 2016, 25(1): 015203 . **doi:** 10.1088/1674-1056/25/1/015203

Out-of-plane shear flow effects on fast magnetic reconnection in a two-dimensional hybrid simulation model

Wang Lin, Wang Xian-Qu, Wang Xiao-Gang, Liu Yue
Chin. Phys. B . 2014, 23(2): 025203 . **doi:** 10.1088/1674-1056/23/2/025203

Basic features of the multiscale interaction between tearing modes and slab ion-temperature-gradient modes*

L Wei(魏来)[1,†], Z X Wang(王正汹)[1,‡], J Q Li(李继全)[2], Z Q Hu(胡朝清)[1], and Y Kishimoto(岸本泰明)[3]

[1] *Key Laboratory of Materials Modification by Laser, Ion, and Electron Beams (Ministry of Education), School of Physics, Dalian University of Technology, Dalian* 116024, *China*

[2] *Southwestern Institute of Physics, Chengdu* 610041, *China*

[3] *Graduate School of Energy Science, Kyoto University, Gokasho, Uji, Kyoto* 611-0011, *Japan*

(Received 24 September 2019; revised manuscript received 30 October 2019; published online 29 November 2019)

Nonlinear interaction between tearing modes (TM) and slab ion-temperature-gradient (ITG) modes is numerically investigated by using a Landau fluid model. It is observed that the energy spectra with respect to wavenumbers become broader during the transition phase from the ITG-dominated stage to TM-dominated stage. Accompanied with the fast growth of the magnetic island, the frequency of TM/ITG with long/short wavelength fluctuations in the electron/ion diamagnetic direction decreases/increases respectively. The decrease of TM frequency is identified to result from the effect of the profile flattening in the vicinity of the magnetic island, while the increase of the frequencies of ITG fluctuations is due to the eigenmode transition of ITG induced by the large scale zonal flow and zonal current related to TM. Roles of zonal current induced by the ITG fluctuations in the instability of TM are also analyzed. Finally, the electromagnetic transport features in the vicinity of the magnetic island are discussed.

Keywords: magnetic reconnection, tearing modes, magnetohydrodynamics, drift waves, nonlinear phenomena

PACS: 52.35.Vd, 52.35.Py, 52.30.Cv, 52.35.Kt **DOI:** 10.1088/1674-1056/ab5437

1. Introduction

Macroscale magnetohydrodynamic (MHD) instabilities, which can induce the global perturbations and thus distort the equilibrium configuration, are dangerous for the steady-state operation of the magnetically controlled fusion devices. Tearing mode (TM), a typical resistive MHD instability, is frequently observed to significantly degrade the plasma confinement in the tokamak plasmas.[1–4] The onset of TMs, especially of the neo-classical TMs, can lead to the fast growth of magnetic island chains by destroying the well-nested magnetic flux surfaces. Hence the TMs inevitably limit the achievable plasma β or even result in the minor or major disruptions, where β is the ratio of thermal pressure to magnetic pressure.

Microscale turbulence, believed to result in the anomalous transports of particles, momentum, and heat in magnetic confinement fusion experiments, is another obstacle for achieving high-performance fusion plasmas. For instance, it has been widely recognized that the ion-scale thermal transport is mainly contributed by the ion-temperature-gradient (ITG) turbulence. There are plenty of evidences that the plasma shear flow plays a critical role in regulating the turbulence and reducing the transport level in the tokamak plasmas.[5,6] Both theoretical and experimental studies show that the formation of the internal and/or edge transport barriers is directly related to the strong plasma shear flow.[7–14] In particular, zonal flow (ZF), self-generated through a modulational or parametric instability of the Reynolds stress of micro-turbulence, can also reduce the saturation amplitude of the micro-turbulence.[15–30]

Usually, the wavelength of the macro-MHD instabilities is approximate to the system size, while the micro-turbulence is in the wavelength range of the Larmor radius which is much smaller than the system size. Due to the difficulties in the experimental diagnosis and the limitations of the computing facilities, many researches only focus on the macro-MHD instabilities or the micro-turbulence transports separately. In the realistic plasmas of fusion devices, however, both the macro-MHD instabilities and the micro-turbulence may coexist and interact with each other.[31–46] On the one hand, the distortion of the magnetic field line and/or the generation of the vortex flow related to the macro-MHD instabilities can modify the onset threshold of the micro-instability and then change the relevant transport characterizations of micro-turbulence. For instance, the parallel transport due to "tearing" magnetic flux surfaces by the unstable TM can flatten the pressure profile, and thus can decrease the drives of the interchange/ITG turbulence as well as the corresponding turbulent transport. On the other hand, anomalous diffusivity due to the micro-turbulence

*Project supported by the National Key R&D Program of China (Grant Nos. 2017YFE0301100 and 2017YFE0300500), the National Natural Science Foundation of China (Grant Nos. 11675038, 11775069, and 11305027), and the Fundamental Research Funds for the Central Universities of China (Grant No. DUT17RC(4)54).

†Corresponding author. E-mail: laiwei@dlut.edu.cn

‡Corresponding author. E-mail: zxwang@dlut.edu.cn

© 2019 Chinese Physical Society and IOP Publishing Ltd

can change the linear growth rate and nonlinear characterizations of the macro-MHD instabilities. For instance, the onset threshold, the growth rate, the mode frequency, and the saturation amplitude of the TMs are all dependent on the strength of the interchange or ITG turbulence.

Aiming to study the multi-scale interactions between ion-scale ITG turbulence and macro-scale TMs, the static magnetic island[47–51] and/or vortex flow[52] related to the tearing instabilities have been embedded in the ITG turbulence by means of gyro-kinetic or Landau fluid simulations. By neglecting the profile flattening effect of the magnetic island, it is found that in the linear regime, the mode structure of ITG is mainly localized near the O-point of the magnetic island due to the geometrical coupling caused by the embedded long wavelength magnetic perturbation of the islands.[47,48] However, once considering the flattening of the pressure profile inside the island, the mode structure of ITG is enhanced at the separatrix of the island but weakened at the O-point of the island.[49] In a gyro-kinetic framework, modifications of the equilibrium profile due to the small island were theoretically analyzed by Wilson and Connor.[53] It is also indicated that in the presence of island, the ITG mode structure is localized along the island direction. Moreover, the effect of the electrostatic turbulence on magnetic islands has been numerically analyzed by Waelbroeck *et al.*[54] Reduction of the propagation velocity of the island due to the turbulence is found to destabilize the thin islands but stabilize the islands whose width is greater than a few times Larmor radius.

Recently, direct nonlinear multi-scale interactions between macro-MHD instabilities and micro-turbulence have been investigated numerically. Li *et al.* found an oscillatory ZF and a magnetic island seesaw phenomenon during the nonlinear interplay between TM and ITG by adopting a slab electromagnetic Landau-fluid model.[55,56] In a kind of art gyro-kinetic framework, Hornsby *et al.* numerically found that the turbulence intensity is much larger at the X-point than that at the O-point of the islands.[57] Ishizawa and Nakajima studied the multi-scale interaction between micro-turbulence and double TM in the reversed magnetic shear configuration by means of a reduced two-fluid simulation.[58] Moreover, Agullo *et al.* carried out a two-dimensional simulation on the characteristic of the magnetic islands driven by an interchange turbulence.[59]

In this work, the nonlinear interplay between drift TM and ITG modes is investigated by using an electromagnetic Landau-fluid model in a sheared slab geometry. A typical transition from ITG dominated stage to TM dominated stage is numerically observed. The spatiotemporal evolution characteristics and the frequency chirp phenomenon during the transition phase are systematically analyzed. Effects of zonal current induced by the ITG fluctuations on the drift TM instability and role of shear flow induced by TM in the eigenmode transition of ITG are both discussed. The electromagnetic transport features in the vicinity of the magnetic island are presented finally.

The remainder of this paper is organized as follows. In Section 2, the modeling equations of an electromagnetic Landau-fluid model are introduced. We present and analyze the numerical results in Section 3. Then, the main results are summarized and discussed in Section 4.

2. Modeling equations

A set of reduced electromagnetic Landau-fluid equations in a sheared slab geometry is employed to study the multi-scale nonlinear interplay between drift TM and ITG modes in this work.[55,56] It includes the plasma density n, electrostatic potential ϕ, parallel component of magnetic vector potential ψ, parallel ion velocity $v_{||}$, and ion temperature $T_{\rm i}$. The quasi-neutral condition is used for the ions and electrons, i.e., $n_{\rm e} \simeq n_{\rm i} \simeq n$. The electron temperature is assumed to be $T_{\rm e0} = \tau T_{\rm i0}$ with τ being a ratio of electron and ion initial temperatures. The normalized equations can be written as

$$\begin{aligned}
{\rm d}_t n &= -\partial_y\phi - \nabla_{||}v_{||} + \nabla_{||}j_{||} + D_n\nabla_\perp^2 n, && (1)\\
{\rm d}_t U &= (1+\eta_{\rm i})\partial_y U + \nabla_{||}j_{||} + D_U\nabla_\perp^2 U, && (2)\\
\beta\partial_t\psi &= -\nabla_{||}(\phi - n) - \beta\partial_y\psi - \eta\, j_{||} + E_0 \\
&\quad + \sqrt{\pi m_{\rm e}/2m_{\rm i}}\,\big|\nabla_{||}\big|\,(v_{||} - j_{||}), && (3)\\
{\rm d}_t v_{||} &= -2\nabla_{||}n - \nabla_{||}T_{\rm i} - \beta(2+\eta_{\rm i})\partial_y\psi + D_v\nabla_\perp^2 v_{||}, && (4)\\
{\rm d}_t T_{\rm i} &= -\eta_{\rm i}\partial_y\phi - \frac{2}{3}\nabla_{||}v_{||} - \frac{2}{3}\sqrt{8/\pi}\,\big|\nabla_{||}\big|\,T_{\rm i} + D_T\nabla_\perp^2 T_{\rm i}, && (5)
\end{aligned}$$

with the operators ${\rm d}_t = \partial_t + \hat{e}_z\times\nabla_\perp\phi\cdot\nabla_\perp$, $\nabla_{||} = \boldsymbol{b}\cdot\nabla$, and $\nabla_\perp^2 = \partial_x^2 + \partial_y^2$. In these equations, $U = \nabla_\perp^2\phi$ is the vorticity and $j_{||} = -\nabla_\perp^2\psi$ is the plasma current density. Equation (2) is derived from the Faraday's law and Ohm's law. The first term of the right-hand side of this equation $-\nabla_{||}\varphi$ is related to the $\boldsymbol{E}\times\boldsymbol{B}$ drift. The second and third terms

$$\begin{aligned}
\nabla_{||}\tilde{n} - \beta\partial_y\tilde{\psi} &= \nabla_{||}\tilde{n} - \beta L_n\,[n_0, \tilde{\psi}] = \left(\bar{\nabla}_{||} + \tilde{\nabla}_{||}\right)\tilde{n} + \tilde{\nabla}_{||}n_0(x)\\
&= \left(\bar{\nabla}_{||} + \tilde{\nabla}_{||}\right)(\tilde{n} + n_0(x)) = \nabla_{||}n_{\rm total}
\end{aligned}$$

are originally from the electron diamagnetic drift (here $\bar{\nabla}_{||}n_0(x) = 0$, since the initial magnetic field is along the y-direction and the density is only a function of x). The density is normalized through $L_n/\rho_{\rm i}\cdot\frac{n}{n_0(x=0)} \to n$ with $L_n^{-1} = -\,{\rm d}\ln n_0/{\rm d}x$ being the typical length of the density gradient. In this reduced model, the electron temperature is assumed to be a constant, so the contribution of the electron temperature gradient to the electron diamagnetic drift is neglected.

The Landau fluid equations employed in this work contain the ion temperature equation with Hammett–Perkins closure.[60] The electron Landau damping effect[61] is included in the last term of Eq. (2). The source term $E_0 = \eta\, j_{||0}$

in Eq. (3) is chosen to balance the diffusion of the initial Ohm current. The initial magnetic field can be expressed as $\boldsymbol{B}_0 = B_0\hat{e}_z - \beta\hat{e}_z \times \nabla_\perp \psi_0 = B_0\hat{e}_z + s\lambda \arcsin h\left(\frac{x}{\lambda}\right)\hat{e}_y$ with constant B_0 along the z-direction. Here, the plasma beta $\beta = 2\mu_0 n_0 T_{i0}/B_0^2$, s is the magnetic shear near the resonant surface, and λ is the gradient length of the initial current layer. In the slab geometry, the uniform gradient of density $L_n^{-1} = -\mathrm{d}\ln n_0/\mathrm{d}x = C$ is assumed. The parameter $\eta_i = \partial \ln T_{i0}/\partial \ln n_{i0}$, which measures the strength of the local ITG mode, is also set to be a constant. The growth rate of tearing mode is proportional to the plasma resistivity η. D_n, D_U, D_v, and D_T are the coefficients of the classical cross-field dissipations. Here, the normalizations are

$$\left\{\frac{x}{\rho_i}, \frac{y}{\rho_i}, \frac{z}{L_n}, \frac{v_{ti}t}{L_n}\right\} \to \{x, y, z, t\},$$
$$L_n/\rho_i \cdot \left\{\frac{e\phi}{T_{i0}}, \frac{2\psi}{\beta B_0 \rho_i}, \frac{n}{n_0}, \frac{v_{||}}{v_{ti}}, \frac{T_i}{T_{i0}}\right\} \to \left\{\phi, \psi, n, v_{||}, T_i\right\},$$

where $\rho_i = v_{ti}/\omega_{ci}$, $v_{ti} = \sqrt{T_0^{rs}/m_i}$, $\omega_{ci} = eB_0/m_i$.

The vorticity equation and the ion temperature equation used in this work are originally from the Refs. [62] and [63]. The Hammett–Perkins closure[60] for the parallel heat flux term and the cancellations that occur between the FLR momentum heat flows and the diamagnetic velocity fluxes have been used in the modeling equations. In the electrostatic limit with adiabatic electrons response, this model can be reduced to the ion Landau fluid model in the shear slab geometry which can be used to study the electrostatic ITG mode. On the other hand, if the drift terms and Landau damping term are neglected, the equations of vorticity and parallel component of the magnetic vector potential become the conventional incompressible 2-field MHD equations which have been widely used to study the resistive tearing modes.

By applying the periodic boundary conditions in the y directions, the perturbed fields can be Fourier-transformed as

$$\tilde{f}(x, y, t) = \frac{1}{2}\sum\nolimits_m \tilde{f}_m(x, t)\exp(\mathrm{i}2\pi m y/Ly) + \mathrm{c.c.}$$

In a shear slab geometry, the zero-boundary condition is used in the x direction for fluctuations with $k_y \neq 0$, i.e., the perturbed fields are set to be zero at the boundary except for the zonal components. The zonal components at the x boundary are set to satisfy the free boundary condition, i.e., $\partial_x \tilde{f}_{k_y=0}(x, t) = 0$, to keep the profile relaxation in the nonlinear simulation. Then, equations (1)–(5) can be solved by an initial value problem (IVP) code in the simulation domain of $L_x = 60\rho_i$ and $L_y = 40\pi\rho_i$. Two-step predictor–corrector method, finite difference method, and pseudo-spectral method are used in the time advancement, the x and y directions, respectively. The grid number in the x direction is set as $N_x = 1024$. The spectral method used in the y direction can easily help us to analyze the mode coupling process between multi-scale interactions. In the nonlinear simulation, the initial perturbations $\tilde{f}_{k_y}(x)$ for all the k_y modes are set to be random functions with small amplitudes. The nonlinear simulations are performed by setting the parameters $s = 0.2$, $\lambda = 2.5$, $\eta_i = 1.5$, $\beta = 0.01$, $\eta = 1.1 \times 10^{-4}$, and $D_n = D_U = D_v = D_T = D = 1 \times 10^{-2}$ for simplicity.

Based on the linear eigenmode analysis for these parameters, the TM is found to be unstable for the fundamental harmonic wave with wave number $\rho_i k_y^{m=1} = 2\pi\rho_i/L_y = 0.05$, linear growth rate $\gamma_{k_y\rho_i=0.05}^{m=1} \approx 9.0 \times 10^{-3}$, and mode frequency $\omega_{k_y\rho_i=0.05}^{m=1} \approx 4.25 \times 10^{-3}$ normalized by the electron diamagnetic drift frequency. The maximum harmonic m_{max} is selected to ensure that $k_y \in [2\pi/L_y, 2\pi m_{max}/L_y]$ can cover all the typical unstable ITG modes. The linear growth rate and mode frequency of the dominant unstable ITG mode are $\gamma_{k_y\rho_i=0.5}^{m=10,l=1} \approx 3.05 \times 10^{-2}$ and $\omega_{k_y\rho_i=0.5}^{m=10,l=1} \approx -0.277$ in the ion diamagnetic drift direction. Here, l corresponds to the radial eigen-function of ITG mode $\hat{\phi}^{(l)}(x)$, which is expressed by the l-th Hermite function.[62,64] Since the linear growth rate of the dominant ITG mode is larger than that of the tearing mode, the tearing mode can grow up after the ITG mode is saturated. Note that the ITG modes with other l are also unstable but they have relatively smaller growth rates and different frequencies. For instance, the linear growth rate and mode frequency of the ITG mode with $k_y\rho_i = 0.5$ and $l = 0$ are $\gamma_{k_y\rho_i=0.5}^{m=10,l=0} \approx 2.96 \times 10^{-2}$ and $\omega_{k_y\rho_i=0.5}^{m=10,l=0} \approx -0.126$. Moreover, in the relatively large magnetic shear regime, the ITG-threshold is higher for the higher radial eigenmode number l, which is consistent with the gyrokinetic prediction in a sheared slab geometry.[65] However, in the weak magnetic shear regime, the dominating unstable ITG mode is usually the mode with higher l.[66]

Since the electromagnetic Landau-fluid equations used here do not include the toroidal effect and kinetic effect except for a fluid closure approximation of Landau damping. Thus, this reduced fluid model could not quantitively give the exact transport level.[67,68] This work mainly focuses on the basic nonlinear multiscale interaction between the macroscale tearing modes with dominating wavenumber $k_y\rho_i = 0.05$ and short wavelength slab ITG modes with dominating wavenumber $k_y\rho_i = 0.5$. The curvature effect in the toroidal geometry[69,70] is not considered in this shear slab model. Thus, the reduced model adopted in this work somewhat limits the application of the results to the curvature-driven interchange modes in the high confinement discharges. More exact kinetic descriptions in the toroidal geometry need further investigation.

3. Numerical results

In this section, the nonlinear interaction between drift TMs and ITG modes is numerically investigated. Firstly, the nonlinear features of wavenumber spectra and frequency spectra of typical TM and ITG modes are given and analyzed. The physical mechanism of the frequency chirping during the transition from the ITG-dominated stage to TM-dominated stage

is identified. Secondly, the roles of zonal flow and zonal current in the multiscale interaction between drift TMs and ITG modes are studied. Finally, the electromagnetic transport features around the magnetic island are discussed.

3.1. Typical features of the drift tearing mode in the ITG turbulence

Aiming to investigate the nonlinear evolution of drift TM in the ITG turbulence, the linear growth rate of the dominating ITG mode is set to be larger than that of the tearing mode by adjusting the initial profiles and parameters in the modeling equations (1)–(5). The linear growth rates of the dominantly unstable tearing mode with $k_y\rho_i = 0.05$ and ITG mode with $k_y\rho_i = 0.5$ are $\gamma^{m=1}_{k_y\rho_i=0.05} \approx 9.0\times10^{-3}$ and $\gamma^{m=10,l=1}_{k_y\rho_i=0.5} \approx 3.05\times10^{-2}$, respectively, as stated in Section 2.

Time evolutions of the magnetic and kinetic energies for the zonal component with $k_y\rho_i = 0$, the long wavelength mode with $k_y\rho_i = 0.05$, and the short wavelength mode with $k_y\rho_i = 0.5$ are presented in Figs. 1(a) and 1(b), respectively. In the linear phase $t < 1\times10^3$, the ITG modes grow exponentially. It is worth noting that the linear growth rate of ITG mode with $k_y\rho_i = 0.5$ and $l = 0$ is $\gamma^{m=10,l=0}_{k_y\rho_i=0.5} \approx 2.96\times10^{-2}$, which is a little smaller than that of the dominant unstable $l = 1$ ITG mode but much larger than those of other higher $l \geqslant 2$ ITG modes, i.e., $\gamma^{m=10,l\geqslant2}_{k_y\rho_i=0.5} \ll \gamma^{m=10,l=0}_{k_y\rho_i=0.5} \leqslant \gamma^{m=10,l=1}_{k_y\rho_i=0.5} \approx 3.05\times10^{-2}$. Thus, both $l = 0$ and $l = 1$ ITG modes can coexist in the early linear growth phase. This can be verified by comparing the normalized k_x spectra of $\tilde{\varphi}(t)$ with $k_y\rho_i = 0.5$ and the eigenfunctions $\hat{\phi}^{(l)}(x)$ for different l. As shown in Fig. 2(b), an oscillation behavior can be observed for the normalized k_x spectra of $\tilde{\varphi}(t < 800)$ during the linear growth phase. The corresponding feature is consistent with the coexistent state of the $l = 0$ and $l = 1$ ITG eigenmodes, according to the normalized k_x spectra of the $l = 0$ and $l = 1$ linear ITG eigenmodes shown in Fig. 2(c). However, after the zonal flow generated by the ITG fluctuations exceeds a certain level, the cascading effect due to the zonal flow is clearly observed during $800 < t < 1000$. Then, the short wavelength ITG fluctuations become saturate in the following phase $1000 < t < 9000$. In this phase, as shown in Fig. 2(a), the $l = 0$ ITG fluctuation with even parity is suppressed. While the $l = 1$ ITG mode with odd parity survives and becomes the dominant one.

Although the growth rate of the long wavelength TM is relatively smaller than that of the dominating ITG modes, the saturation amplitude of macro-TM is larger than that of ITG modes. Thus, a transition phase from the ITG-dominated stage to TM-dominated stage is clearly observed in the time interval $9\times10^3 < t < 1.1\times10^4$. During this transition phase, the magnetic energy with $k_y\rho_i = 0.05$ grows abruptly, accompanied with the formation of the magnetic island. It is found that the k_y spectra of both kinetic and magnetic energies become broader after the transition, as shown in Figs. 1(c) and 1(d). Moreover, it should be noted that the zonal field in Fig. 1(d), which is generated by the electromagnetic ITG fluctuations, can weaken the magnetic shear near the resonant surface. Roles of the zonal current related to the zonal field in the nonlinear interaction process will be discussed in the next section.

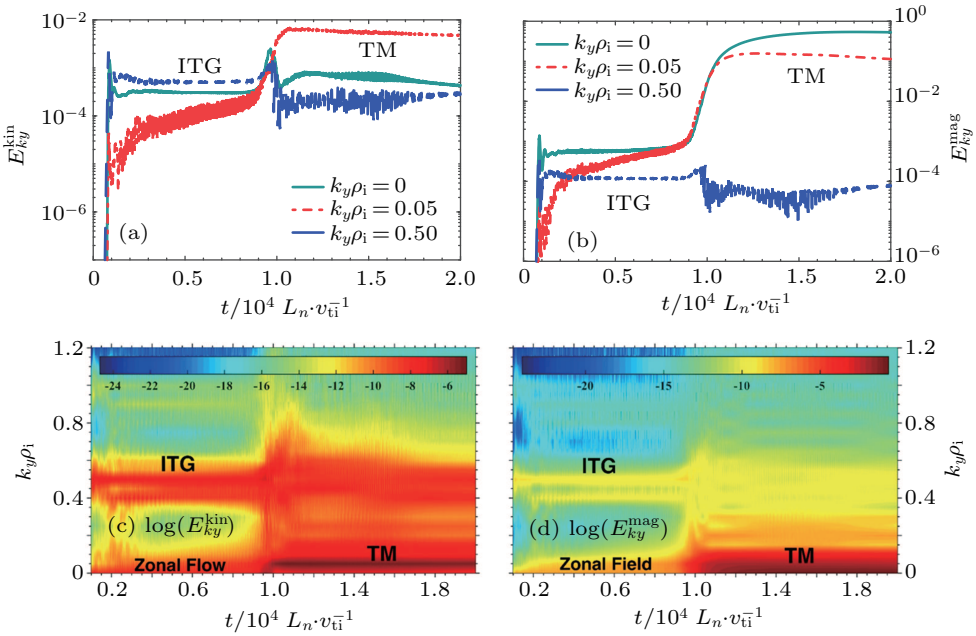


Fig. 1. Time evolution of (a) the kinetic E^{kin}_{ky} and (b) magnetic E^{mag}_{ky} energies for the zonal component with $k_y\rho_i = 0.0$, long wavelength tearing mode with dominating wavenumber $k_y\rho_i = 0.05$, and short wavelength ITG modes with dominating wavenumber $k_y\rho_i = 0.5$. Instantaneous k_y spectra for (c) the kinetic and (d) magnetic energies in the log scale. Here, $E^{kin}_{ky} = \frac{1}{2}\left\langle\left|\nabla\tilde{\phi}_{ky}\right|^2\right\rangle = \frac{1}{2}\int_{-Lx}^{Lx}\nabla\tilde{\phi}_{ky}\cdot\nabla\tilde{\phi}^*_{ky}\mathrm{d}x$ and $E^{mag}_{ky} = \frac{1}{2}\left\langle\left|\nabla\tilde{\psi}_{ky}\right|^2\right\rangle = \frac{1}{2}\int_{-Lx}^{Lx}\nabla\tilde{\psi}_{ky}\cdot\nabla\tilde{\psi}^*_{ky}\mathrm{d}x$ are, respectively, the average kinetic and magnetic energies of the fluctuations for different k_y.

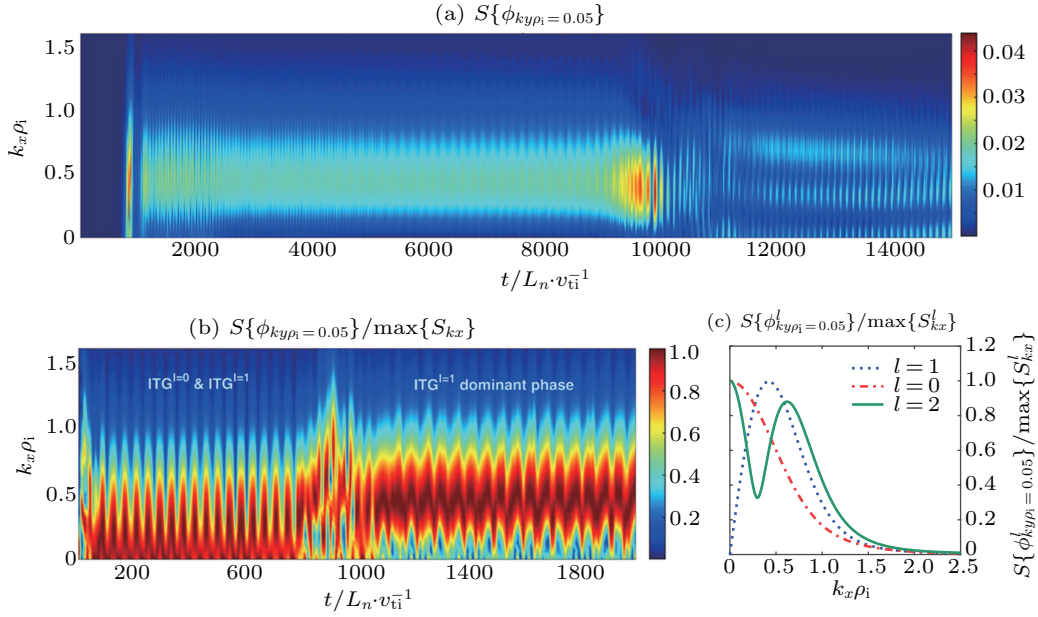


Fig. 2. (a) Instantaneous k_x spectra of the potential $\tilde{\varphi}_{ky=0.5}$. (b) Normalized k_x spectra of the potential $\tilde{\varphi}_{ky=0.5}$ during $t \in [0, 2000]$. (c) Normalized k_x spectra of the linear ITG eigenmode $\hat{\varphi}^l_{ky=0.5}$ with $l = 0, 1, 2$. The k_x spectra shown in these figures are obtained through the Fourier-transform of $\tilde{\phi}_{ky}(x)$.

Time evolutions of the frequency spectra for TM with $k_y\rho_i = 0.05$ and ITG mode with $k_y\rho_i = 0.5$ are given in Fig. 3. The eigen-frequencies of TM and ITG modes obtained by an eigenvalue problem solver are also indicated in Figs. 3(a) and 3(b) with dash-dot lines. The frequencies of TM and ITG modes, normalized by the electron diamagnetic drift frequency, are positive and negative, respectively. During the transition phase, the generation of the magnetic island provides a short cut for the particle and energy transport, which results in the flattening of the plasma profile. Therefore, the electron diamagnetic frequency decreases near the island region. Then the rotation of TM gradually slows down during the transition phase, as shown in Fig. 3(a). At the same time, the frequency chirping of the ITG modes is also observed, as shown in Fig. 3(b).

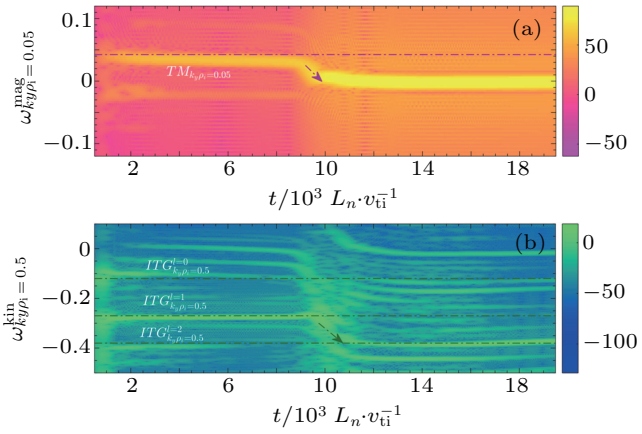


Fig. 3. Frequency Spectra for the (a) long wavelength tearing mode with $k_y\rho_i = 0.05$ and (b) short wavelength ITG modes with $k_y\rho_i = 0.5$. The background color indicates the frequency spectral density of the potential near the resonant surface $\tilde{\varphi}(x \approx 0)$. The frequencies of the eigenmodes for the initial profiles are also indicated with dash-dot lines.

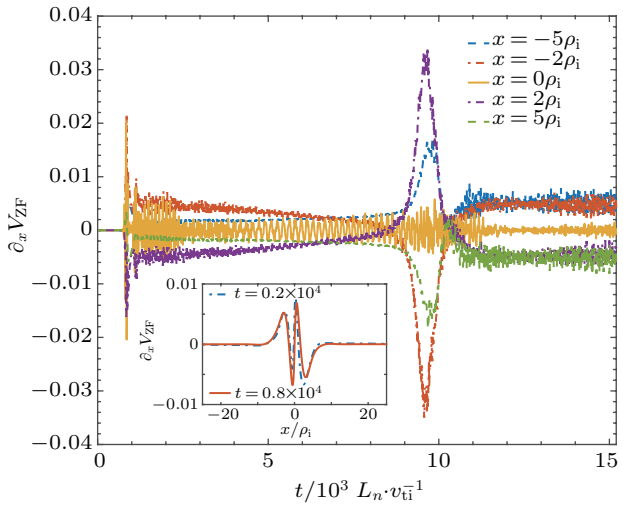


Fig. 4. (a) Time history of the shear rate of zonal flow $\partial_x V_{ZF}(t)$ near the resonant surface ($x = 0, \pm 2\rho_i, \pm 5\rho_i$). Inset: shear profiles of zonal flow $\partial_x V_{ZF}(x)$ at different time.

It is noted that before the transition, the fluctuations induced by the ITG modes are relatively small compared to fluctuations in the tearing mode dominated stage. Thus, the amplitude of the shear rate of the zonal flow is relatively weak, as shown in Fig. 4. The frequency of the tearing modes only weakly deviates from the electron diamagnetic drift before the transition, as shown in Fig. 3. During the transition, the zonal flow grows very fast near $t = 0.95 \times 10^4$, accompanying with the fast growth of the magnetic island. The electron diamagnetic drift flow also decreases very fast due to the flattened profile near the island region. Time evolution of the zonal flow and electron diamagnetic drift flow is given in Fig. 5. It is inferred that the fast frequency sweeping down in Fig. 3(a) is mainly because of the combination effect of the zonal flow and electron diamagnetic drift.

Near $t = 1400$, "predator–prey" behavior of the zonal flow and ITG fluctuations occurs. In the initial stage, the unstable ITG modes grow exponentially, which drives the growth of the zonal flow, as indicated in Fig. 5. When the zonal flow generated by the ITG fluctuations exceeds a certain level, the ITG fluctuations decrease due to the shear rate of the zonal flow. Then, the drive term of zonal flow becomes weak. The viscosity leads to the damping of the zonal flow. This process can be clearly observed in the phase-relation between ITG fluctuations and zonal flow shown in Fig. 6. Moreover, it is found that the shear of ZF near $x = 0$ is oscillating during the ITG dominated stage, as shown in Fig. 4. This is mainly because of the nonlinear coupling effect between the ITG modes with odd and even parities.

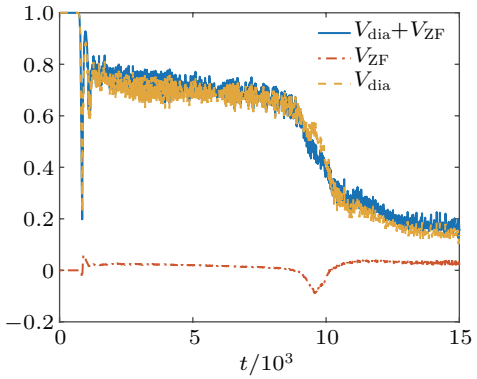


Fig. 5. Time evolution of the zonal flow and electron diamagnetic drift electron diamagnetic drift at the resonant surface $x = 0$.

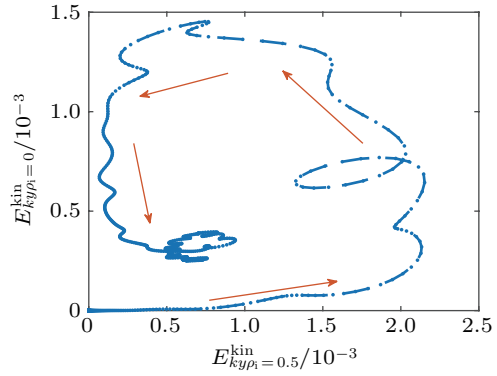


Fig. 6. The phase-relation between ITG fluctuations and zonal flow during $t \in [0, 1500]$.

The increase of the frequencies of ITG fluctuations is mainly because of the eigenmode transition. This can be verified by the mode structure variation during the transition phase. As shown in Fig. 7, in the transition phase, the amplitude of the odd parity ITG mode with $l = 1$ decreases, while the even parity ITG modes with $l \geqslant 2$ grow up. Since the eigen frequency of the ITG mode increases with the radial wavenumber, the eigenmode transition from the $l = 1$ odd ITG mode to $l \geqslant 2$ even ITG modes directly leads to the frequency chirping shown in Fig. 3(b). The underlying mechanism is similar to the mode transition of the multiple eigenmodes of the toroidal ITG instabilities, which were observed in the very recent gyrokinetic simulations.[71,72]

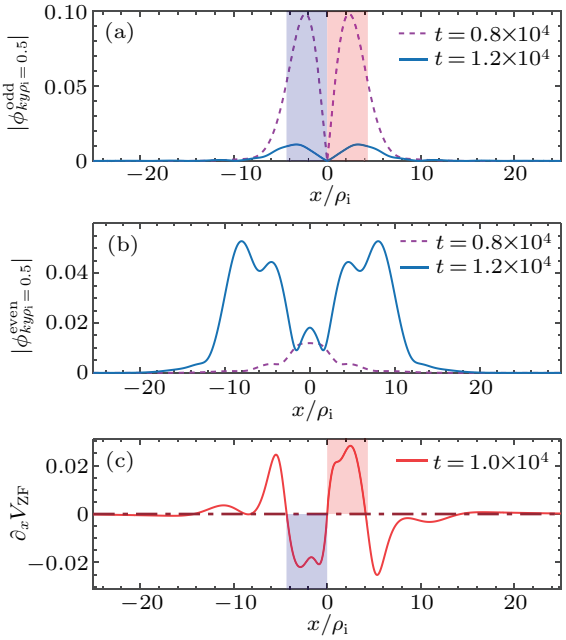


Fig. 7. (a) Odd and (b) even parities of the absolute value of the ITG modes $|\tilde{\phi}|$ with $k_y\rho_{\rm i} = 0.5$ at $t = 0.8 \times 10^4$ (before transition) and $t = 1.2 \times 10^4$ (after transition). (c) Shear of the zonal flow profile $\partial_x V_{\rm ZF}$ at $t = 0.8 \times 10^4$ (during transition).

Moreover, the two sweeping-down belts around $\omega \approx 0$ and $\omega \approx -0.05$ in Fig. 3(b) are originally from the mode coupling effect between the tearing modes and ITG modes. As shown in Fig. 8(a), the mode frequency of the second harmonic tearing mode with $k_y^{m=2}\rho_{\rm i} = 0.1$ is around $\omega^{m=2,{\rm TM}}_{k_y\rho_{\rm i}=0.1} \approx 0.07$ in the electron diamagnetic drift direction. While, the ITG mode with $k_{k_y}^{l=0}\rho_{\rm i} = 0.4$ is around $\omega^{m=8,l=0}_{k_y\rho_{\rm i}=0.4} \approx -0.07$ in the ion diamagnetic drift direction, as shown in Fig. 8(b). Thus, the sweeping-down belt before the transition around $\omega \approx 0$ is originally from the mode coupling between the tearing mode with $k_y^{m=2}\rho_{\rm i} = 0.1$ and ITG mode with $k_{k_y}^{l=0}\rho_{\rm i} = 0.4$, i.e., $\omega^{m=2,{\rm TM}}_{k_y\rho_{\rm i}=0.1} + \omega^{m=8,l=0}_{k_y\rho_{\rm i}=0.4} \approx 0$.

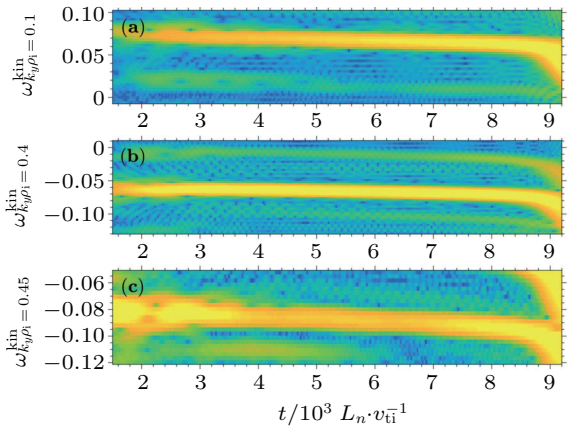


Fig. 8. Frequency spectra for (a) $k_y\rho_{\rm i} = 0.1$, (b) $k_y\rho_{\rm i} = 0.4$, and (c) $k_y\rho_{\rm i} = 0.45$.

Similarly, the sweeping-down belt before the transition around $\omega \approx -0.05$ in Fig. 3(b) is originally from the mode coupling between the tearing mode with $k_y\rho_i = 0.05$ and ITG mode with $k_{k_y}^{l=0}\rho_i = 0.45$. As shown in Fig. 3(a), the frequency of the tearing mode with $k_y\rho_i = 0.05$ is around $\omega_{k_y\rho_i=0.05}^{m=1,\mathrm{TM}} \approx 0.04$. The ITG mode with $k_{k_y}^{l=0}\rho_i = 0.45$ is around $\omega_{k_y\rho_i=0.45}^{m=9,l=0} \approx -0.09$, as shown in Fig. 8(c). Thus, $\omega_{k_y\rho_i=0.05}^{m=1,\mathrm{TM}} + \omega_{k_y\rho_i=0.45}^{m=9,l=0} \approx -0.05$.

3.2. Dynamics of the zonal flow and zonal current during the transition

The change of the zonal flow and current profile from the ITG dominated stage to TM dominated stage can help to understand the eigenmode transition from the $l = 1$ odd ITG mode to $l \geqslant 2$ even ITG modes. According to the time history of the zonal flow and current profiles presented in Fig. 9, the amplitudes of the zonal flow and its shear rate become large during the transition phase. The zonal flow in the TM dominated stage is broader than the zonal flow driven by the ITG fluctuations. The shear rate of the zonal flow profile during the transition phase is plotted in Fig. 7(c). It is found that the two peak points of the ITG fluctuation with odd parity are just located in the large shear region of the zonal flow. Thus, it can be inferred that the increase of the zonal flow due to the tearing activity leads to the suppression of the $l = 1$ ITG mode. However, as shown in Fig. 7(b), the $l \geqslant 2$ ITG modes are excited due to the collapse of the current profile by the macro-TM instability. Before the transition, the zonal current generated from the ITG fluctuations is localized near the resonant surface. Because the direction of the zonal current induced by the ITG fluctuations is opposite to that of the initial current, the total current density decreases near the resonant surface. Thus, it is observed that a cave of the current density is formed at $x = 0$, as shown in Fig. 9 and the inset of Fig. 10 with blue dash-dot line. Therefore, the magnetic shear $s = \langle \partial_x B_y \rangle = \langle J_z \rangle$ decreases near the resonant surface. It is found that the current density or the magnetic shear decreases nearly 6.5% in the ITG-dominated stage. However, during the transition phase, the fast growth of the tearing mode leads to the current profile collapse. The current density or magnetic shear decreases almost 45% of the initial current density or magnetic shear during the transition phase. As shown in the inset of Fig. 10 with green dot line, the current profile becomes flat in the TM-dominated stage, which can excite the ITG mode with higher l and higher frequency in the ion diamagnetic direction. The enhancement of the broader spectra near $t = 9500$ shown in Figs. 1 and 2 also verifies the destabilization of the ITG modes with different l. Moreover, as stated above, the $l = 1$ ITG fluctuation can be suppressed effectively by the shear of the zonal flow during the transition phase. Thus, it can be inferred that the destabilization of the ITG modes with different l and the suppression of the previous dominant $l = 1$ ITG fluctuations result from the combined effects of the zonal field and zonal flow due to the fast growth of the long wavelength perturbation induced by the tearing mode.

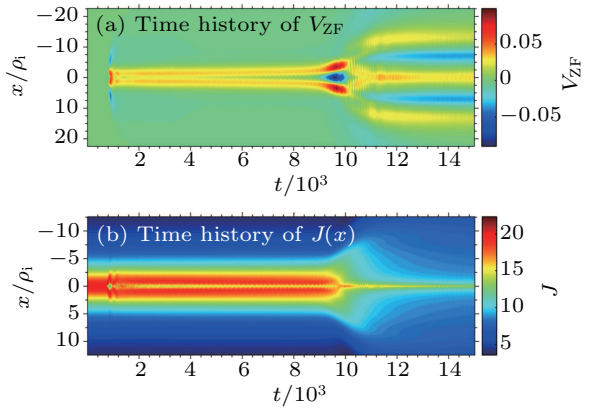


Fig. 9. Time history of (a) zonal flow $V_{ZF}(x,t)$ and (b) current density $J(x,t)$ profiles.

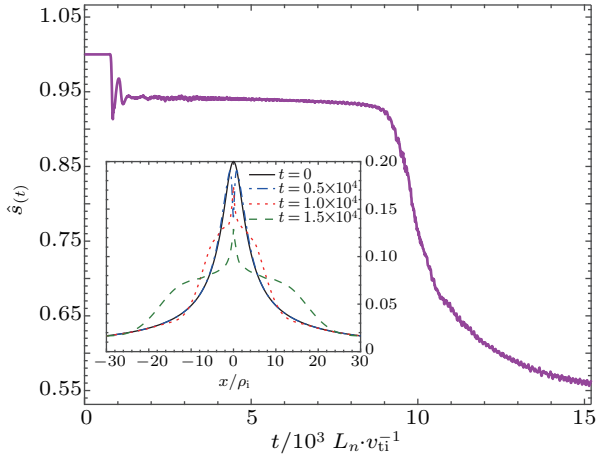


Fig. 10. (a) Time history of the averaged magnetic shear $\hat{s}(t) = \langle s(\bar{x},t)\rangle/s(\bar{x},t=0) = \int_{-1.5\rho_i}^{1.5\rho_i} s(x,t)\mathrm{d}x / \int_{-1.5\rho_i}^{1.5\rho_i} s(x,t=0)\mathrm{d}x$ near the resonant surface $\bar{x} \in [-1.5\rho_i, 1.5\rho_i]$. Inset: magnetic shear profiles $s(x)$ at different time.

Therefore, the frequency chirping phenomenon observed during the transition phase is mainly because of the mode transition between the ITG modes with different mode frequencies. The trigger of the mode transition is because of the differences of the zonal flow and zonal field/current generated from micro-ITG and macro-TM, respectively. It is worth noting that the zonal flow can also affect the other ITG modes with different l. As shown in Fig. 7(b), it can be also observed that the amplitude of the even ITG fluctuation is relatively small near the peak region of the zonal flow shear. However, it seems that the ITG modes with relatively lower radial mode numbers are easily suppressed by the zonal flow shear.

Furthermore, it is found that the long wavelength fluctuation can be driven by the short wavelength ITG fluctuations though the nonlinear wave–wave coupling process. However, the zonal field or zonal current generated from the ITG fluc-

tuations can weaken the magnetic shear near the resonant surface, which has a stabilized effect on the long wavelength tearing activity. Thus, several exponential growth phases for the fluctuation with $k_y\rho_i = 0.05$ are shown in Fig. 11. The initial exponential growth phase is according to the linearly unstable TM with growth rate smaller than the growth rate of the short wavelength ITG modes, as indicated with bluish violet interval in Fig. 11. When the amplitude of the ITG fluctuations exceeds a threshold, accompanying with the zonal component, the long wavelength mode driven by the short wavelength ITG mode through wave–wave coupling effect grows exponentially during $t \in [500, 900]$, as indicated with the red line in Fig. 11. In the following phase, the ITG fluctuations are saturated gradually. During this phase $t \in [0.2\times10^{-4}, 0.8\times10^{-4}]$, the zonal current generated from the ITG fluctuations leads to the decrease of the magnetic shear near the resonant surface, as shown in Fig. 10. Since the tearing activity becomes weaker as the magnetic shear decreases, it is observed that the growth rate of the long wavelength mode during $t \in [0.9\times10^{-4}, 1.2\times10^{-4}]$ is much smaller than that of the initial linear growth rate of TM during $t \in [150, 500]$, as shown in Fig. 11. It is noted that even though the change of the magnetic shear due to the zonal current generated from ITG fluctuations is relatively weak, it will play an important role in the marginal unstable TM instability.

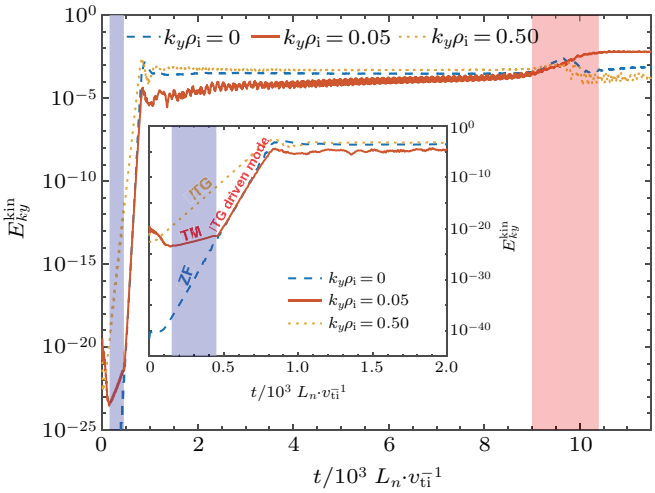


Fig. 11. (a) Time evolution of the kinetic energy E^{kin}_{ky} for the zonal component with $k_y\rho_i = 0.0$, long wavelength tearing mode with dominating wavenumber $k_y\rho_i = 0.05$, and short wavelength ITG modes with dominating wavenumber $k_y\rho_i = 0.5$. Inset: the amplification of (a) in the time interval $t \in [0, 2000]$. Here, $E^{kin}_{ky} = \frac{1}{2}\left\langle\left|\nabla\tilde{\phi}_{ky}\right|^2\right\rangle = \frac{1}{2}\int_{-Lx}^{Lx}\nabla\tilde{\phi}_{ky}\cdot\nabla\tilde{\phi}^*_{ky}\mathrm{d}x$ is the average kinetic energy of the fluctuations for different k_y.

In fact, the magnetic shear in the ITG-dominated stage is influenced by not only the zonal current generated by the ITG fluctuations but also the source term $E_0 = \eta J_0$ chosen to balance the diffusion of the initial current in Eq. (3). Since the source term related to $E_0 \propto \eta$ counteracts the decrease of the magnetic shear induced by the zonal current, it can be found that the mean shear of the magnetic field near the resonant surface increases with increasing resistivity. Thus, in the ITG-dominated stage, it can be inferred that the tearing activity is more easily excited when the source term $E_0 = \eta J_0$ is strong for the same level of the zonal current.

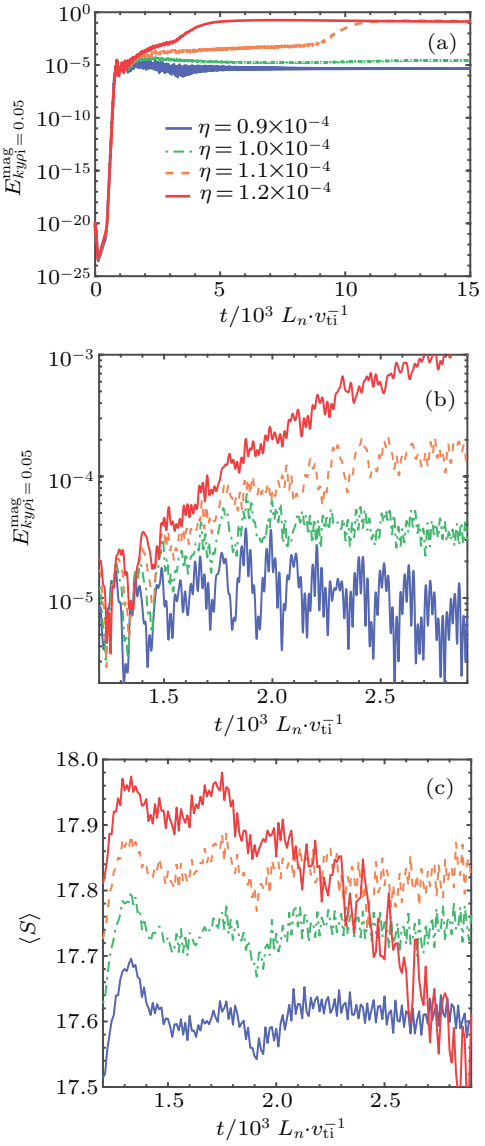


Fig. 12. (a) Time evolution of the magnetic energies for the long wavelength mode with $k_y\rho_i = 0.05$ for various resistivities. (b) The amplification of (a) in the time interval $t \in [1.2\times10^3, 2.9\times10^3]$. (c) Time evolution of the averaged magnetic shear $\hat{s}(t) = \langle s(\bar{x},t)\rangle/s(\bar{x},t=0) = \int_{-1.5\rho_i}^{1.5\rho_i} s(x,t)\mathrm{d}x/\int_{-1.5\rho_i}^{1.5\rho_i} s(x,t=0)\mathrm{d}x$ near the resonant surface $\bar{x} \in [-1.5\rho_i, 1.5\rho_i]$.

Roles of the source term $E_0 = \eta J_0$ in the nonlinear interaction between the tearing mode and ITG modes have been studied by varying the resistivity in this work, since the strength of the source term is proportional to the resistivity for the same current profile. It can be observed in Fig. 12 that, during the ITG-dominated stage, the tearing activity is only excited in the large resistivity regime. Nevertheless, in the small resistivity regime, the tearing activity is stabilized by the zonal current. The fluctuation of the long wavelength mode saturates in the ITG-dominated stage as shown by the

green and blue lines in Fig. 12. Although the temperature gradient driven ITG fluctuations and corresponding zonal current are almost the same in all cases (temperature gradient is set as $\eta_i = 1.5$), the source term proportional to the resistivity is not strong enough to counteract the stabilizing effect of the zonal current generated by the ITG fluctuation in the small resistivity regime. Therefore, the tearing mode becomes stable for $\eta \leqslant 1 \times 10^{-4}$. In the large resistivity regime, however, the decrease of magnetic shear induced by the ITG driven zonal current can be compensated by the strong source term. As shown in Fig. 12(b), the TM begins to grow near $t = 2000$ for $\eta > 1 \times 10^{-4}$. The phenomenon that the magnetic shear near the resonant surface increases with increasing resistivity also supports the pervious conjecture, as shown in Fig. 12(c).

Furthermore, previous studies indicate that the polarization current has a destabilizing effect on the TM when the magnetic island exceeds a critical value.[73,74] It is also observed in Fig. 12 that the long wavelength mode grows suddenly when the amplitude of the magnetic fluctuation reaches a threshold. For example, in the case with resistivity $\eta = 1.1 \times 10^{-4}$ (the orange curve in Fig. 12), the long wavelength mode grows slowly during $t \in [0.2 \times 10^{-4}, 0.8 \times 10^{-4}]$, while it grows rapidly during $0.8 \times 10^{-4} < t < 1.2 \times 10^{-4}$. In fact, this typical case has been used in the spectra analysis in the previous paragraphs. The sudden growth phase is just the transition phase from the ITG dominated stage to the TM dominated stage, as shown in Fig. 1. In the slow growth phase of the TM, the ITG fluctuation is dominant. After the fast growth of the tearing mode, however, the TM gradually becomes dominant in the final state.

3.3. Transport characteristic in the vicinity of the magnetic island

Turbulent transport in the presence of magnetic island has received extensive attention in recent years. Thus, in this work, the transport feature near the island region is also discussed. For the electromagnetic turbulence, the particle and thermal transport is associated directly with the fluctuations of radial velocity $\tilde{v}_x$ and the electromagnetic part $\tilde{b}_x\tilde{v}_\parallel$ due to the magnetic fluctuations. Both $\tilde{v}_x$ and $\tilde{b}_x\tilde{v}_\parallel$ during the transition phase are presented in Fig. 13. In the ITG dominated stage, the magnetic perturbation is relatively weak, since the ITG mode is a typical kind of electrostatic instability. Thus, the turbulent transport is contributed mainly by the electrostatic part $\langle\tilde{v}_x\tilde{n}\rangle$ or $\langle\tilde{v}_x\tilde{T}_i\rangle$. When the TM grows up, the magnetic island gradually splits the small-scale fluctuations. As shown in Figs. 13(a)–13(e), the fluctuations are mainly localized near the magnetic separatrix. As the width of the magnetic island increases, the fluctuations are gradually squeezed to the X-point of the magnetic island. On the other hand,

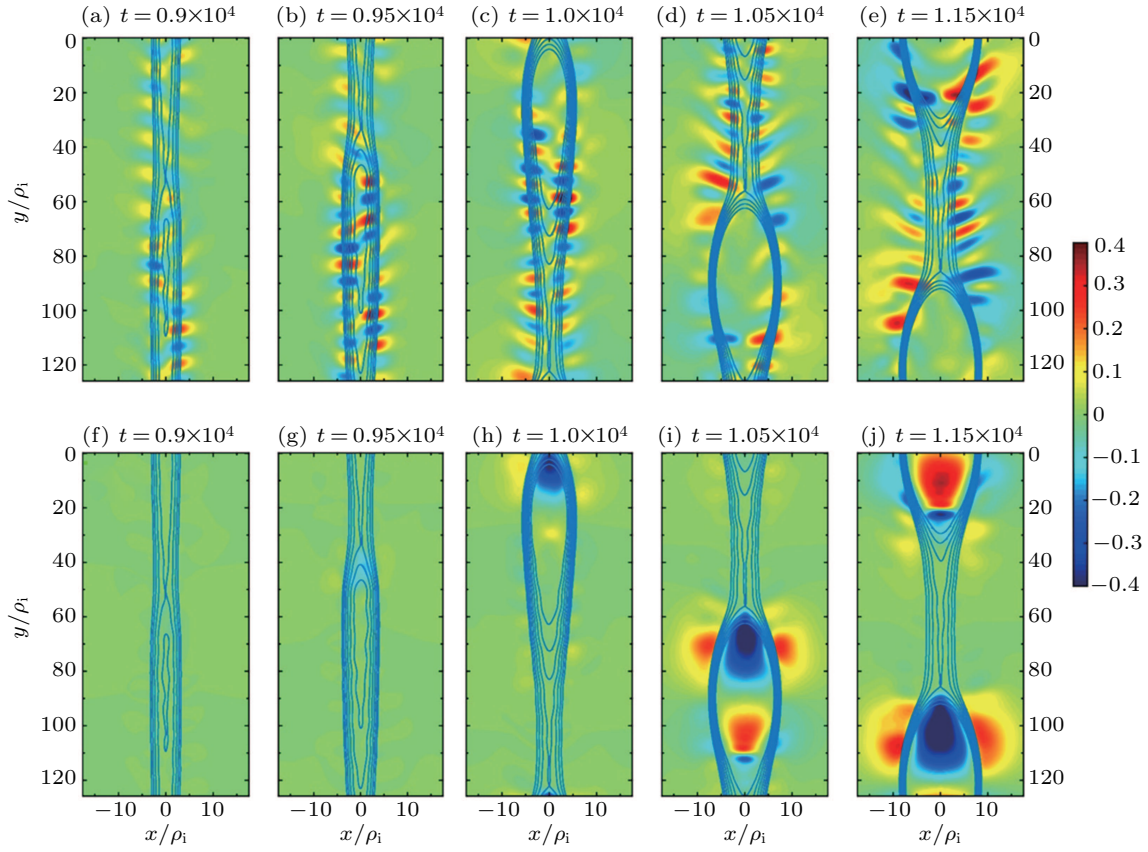


Fig. 13. Snapshots of the velocity fluctuations in the x-direction $\tilde{v}_x$ (top row) and $\tilde{b}_x\tilde{v}_\parallel$ (bottom row) during the transition phase. The contour lines of the magnetic flux near the resonant surface represent the magnetic field lines or corresponding magnetic island. In this case, the resistivity is set to $\eta = 1.1 \times 10^{-4}$.

the fluctuations near the O-point of the magnetic island become very weak. This structure is different from the mode structure of the linear ITG mode in the presence of static magnetic island.[47,48] In the linear regime, the mode coupling effect associated with the magnetic island may lead to the mode structure that is mainly concentrated inside the magnetic island region. In the nonlinear regime, the profiles may be flattened inside the island. The steep gradient outside the magnetic island may enhance the ITG fluctuations around the magnetic separatrix, which is consistent with the phenomenon observed in Figs. 1 and 13. However, the formation of the large-scale vortex flow and corresponding zonal flow related to the tearing mode can suppress the turbulence in the following tearing mode dominated stage. Thus, it can be observed in Fig. 1 that the turbulence intensity firstly increases in the transition phase and then decreases in the following phase. This phenomenon is quantitively similar to the experimental diagnosis in EAST tokamak, as indicated in Fig. 4 of Ref. [75] (In EAST tokamak, it is also observed that the turbulence intensity increases as the width of the magnetic island grows in the transition phase. Then it decreases when the magnetic island saturates).

Moreover, when the magnetic island becomes large, the transport associated with the electromagnetic fluctuation $\tilde{b}_x\tilde{v}_{\parallel}$ cannot be neglected. As shown in Fig. 13(j), the dominating contribution is the long wavelength perturbations, which are associated with the large scale $\tilde{v}_{\parallel}$ and bending of the magnetic field lines around the magnetic island.

4. Summary and discussion

In summary, the typical features of the multiscale interaction between drift tearing mode and ITG modes are investigated by means of an electromagnetic Landau-fluid simulation in a shear slab geometry. A transition phase from the ITG-dominated stage to TM-dominated stage is clearly observed when the initial linear growth of the ITG mode is larger than that of TM. During the transition phase, the energy spectra with respect to wavenumbers become broader. Interestingly, a frequency chirping phenomenon is found during the transition phase. The decrease of the frequency of the long wavelength tearing mode in the electron diamagnetic direction is mainly because of the flattened profile due to the fast growth of the magnetic island. While the increase of the frequencies of the short wavelength ITG fluctuations in the ion diamagnetic direction is because of the eigenmode transition of ITG induced by the large-scale zonal flow and zonal current related to the drift TM. Stabilizing effect of zonal current induced by the ITG fluctuations on the drift TM instability is also analyzed. Finally, the electromagnetic transport features in the vicinity of the magnetic island are discussed. Although the turbulence transport is mainly contributed by the electrostatic part when the magnetic perturbation is small, the transport associated with the electromagnetic fluctuations could not be neglected when the magnetic island becomes large.

It is clarified that for the large magnetic island, the flattening of the pressure profile resulting in the reduction/enhancement of the ITG fluctuation inside/outside the island is found to dominate over the geometrical coupling effect of the island, which leads to the localization of the ITG mode inside the island. As a result, the net effect of the island is an enhancement of the ITG fluctuation near the separatrix of the island, especially near the X-point of the island.

Furthermore, the basic results obtained in this work can help us to understand the experimental diagnosis to a certain degree. For example, the behavior of the turbulence intensity during the transition phase from the ITG-dominated stage to TM-dominated stage in this work is quantitively similar to the experimental diagnosis in EAST tokamak. As indicated in Fig. 4 of Ref. [75], the turbulence intensity increases as the width of the magnetic island grows in the transition phase. Then it decreases when the magnetic island saturates. This phenomenon is similar to the numerical results obtained in Fig. 1(a). The increase of the turbulence identity is mainly because of the steepened temperature profile near the magnetic separatrix. The decrease of the turbulence intensity is mainly because of the vortex flow and zonal flow related to the tearing mode.

The numerical simulation is only carried out based on a reduced Landau-fluid model in a shear slab geometry. The magnetic field-line curvature plays an important role in the toroidal ITG modes. In this work, only local slab-ITG modes interacting with the tearing mode in a shear slab are considered. The results may be different in the toroidal geometry. Moreover, the shear flow/mean flow effect which may modify and/or update this conclusion in some extent is not included in this work. Thus, the influence of curvature and the equilibrium flow on the multi-scale interaction between TM and ITG should be considered in the future.

Acknowledgment

The authors would like to thank Professor X G Wang, Professor J Q Dong, Professor P H Diamond, Professor Y H Xu, and Dr. H S Xie for helpful discussions.

References

[1] Hender T C, Wesley J C, Bialek J, *et al.* 2007 *Nucl. Fusion* **47** S128
[2] Kikuchi M and Azumi M 2012 *Rev. Mod. Phys.* **84** 1807
[3] Porcelli F 1987 *Phys. Fluids* **30** 1734
[4] Wang X and Bhattacharjee A 1993 *Phys. Rev. Lett.* **70** 1627
[5] Doyle E J, Houlberg W A, Kamada Y, *et al.* 2007 *Nucl. Fusion* **47** S18–S127
[6] Horton W 1999 *Rev. Mod. Phys.* **71** 735
[7] Terry P W 2000 *Rev. Mod. Phys.* **72** 109
[8] Lin Z, Hahm T S, Lee W W, Tang W M and White R B 1998 *Science* **281** 1835

[9] Diamond P H, Itoh S I, Itoh K and Hahm T S 2005 *Plasma Phys. Control. Fusion* **47** R35

[10] Shirai H, Kikuchi M, Takizuka T, Fujita T, Koide Y, Rewoldt G, Mikkelsen D, Budny R, Tang W M, Kishimoto Y, Kamada Y, Oikawa T, Naito O, Fukuda T, Isei N, Kawano Y, Azumi M and J T-60 Team 1999 *Nucl. Fusion* **39** 1713

[11] Tala T J J, Heikkinen J A, Parail V V, Baranov Yu F and Kartttunen S J 2001 *Plasma Phys. Control. Fusion* **43** 507

[12] Garbet X, Bourdelle C, Hoang G T and Maget P 2001 *Phys. Plasmas* **8** 2793

[13] Benkadda S, Beyer P, Bian N, Figarella C, Garcia O, Garbet X, Ghendrih P, Sarazin Y and Diamond P H 2001 *Nucl. Fusion* **41** 995

[14] Dong J Q, Mou Z Z, Long Y X and Mahajan S M 2004 *Phys. Plasmas* **11** 5673

[15] Hamaguchi S and Horton W 1992 *Phys. Fluids B* **4** 319

[16] Xu Y H, Yu C X, Luo J R, Mao J S, Liu B H, Li J G, Wan B N and Wan Y X 2000 *Phys. Rev. Lett.* **84** 3867

[17] Dimits A M, Bateman G, Beer M A, Cohen B I, Dorl, W, Hammett G W, Kim C, Kinsey J E, Kotschenreuther M, Kritz A H, Lao L L, Mandrekas J, Nevins W M, Parker S E, Redd A J, Shumaker D E, Sydora R and Weiland J 2000 *Phys. Plasmas* **7** 969

[18] Fujisawa A, Itoh K, Iguchi H, Matsuoka K, Okamura S, Shimizu A, Minami T, Yoshimura Y, Nagaoka K, Takahashi C, Kojima M, Nakano H, Ohsima S, Nishimura S, Isobe M, Suzuki C, Akiyama T, Ida K, Toi K, Itoh S I and Diamond P H 2004 *Phys. Rev. Lett.* **93** 165002

[19] Zhao K J, Lan T, Dong J Q, Yan L W, Hong W Y, Yu C X, Liu A D, Qian J, Cheng J, Yu D L, Yang Q W, Ding X T, Liu Y and Pan C H 2006 *Phys. Rev. Lett.* **96** 255004

[20] Peng X D, Tang C J and Qiu X M 2007 *Phys. Plasmas* **14** 010703

[21] Lan T, Liu A D, Yu C X, Yan L W, Hong W Y, Zhao K J, Dong J Q, Qian J, Cheng J, Yu D L and Yang Q W 2008 *Phys. Plasmas* **15** 056105

[22] Liu A D, Lan T, Yu C X, Zhao H L, Yan L W, Hong W Y, Dong J Q, Zhao K J, Qian J, Cheng J, Duan X R and Liu Y 2009 *Phys. Rev. Lett.* **103** 095002

[23] Xu G S, Wan B N, Wang H Q, Guo H Y, Zhao H L, Liu A D, Naulin V, Diamond P H, Tynan G R, Xu M, Chen R, Jiang M, Liu P, Yan N, Zhang W, Wang L, Liu S C and Ding S Y 2011 *Phys. Rev. Lett.* **107** 125001

[24] Wang Z H, Diamond P H, Gürcan D, Garbet X and Wang X G 2011 *Nucl. Fusion* **51** 073009

[25] Xu M, Tynan G R, Diamond P H, Manz P, Holl, C, Fedorczak N, Chakraborty Thakur S, Yu J H, Zhao K J, Dong J Q, Cheng J, Hong W Y, Yan L W, Yang Q W, Song X M, Huang Y, Cai L Z, Zhong W L, Shi Z B, Ding X T, Duan X R, Liu Y and HL-2A team 2012 *Phys. Rev. Lett.* **108** 245001

[26] Schmitz L, Zeng L, Rhodes T L, Hillesheim J C, Doyle E J, Groebner R J, Peebles W A, Burrell K H and Wang G 2012 *Phys. Rev. Lett.* **108** 155002

[27] Cheng J, Dong J Q, Itoh K, Yan L W, Xu M, Zhao K J, Hong W Y, Huang Z H, Ji X Q, Zhong W L, Yu D L, Itoh S I, Nie L, Kong D F, Lan T, Liu A D, Zou X L, Yang Q W, Ding X T, Duan X R, Liu Y and HL-2A team 2013 *Phys. Rev. Lett.* **110** 265002

[28] Tynan G R, Xu M, Diamond P H, Boedo J A, Cziegler I, Fedorczak N, Manz P, Miki K, Thakur S, Schmitz L, Zeng L, Doyle E J, McKee G M, Yan Z, Xu G S, Wan B N, Wang H Q, Guo H Y, Dong J, Zhao K, Cheng J, Hong W Y and Yan L W 2013 *Nucl. Fusion* **53** 073053

[29] Kobayashi S, Gürcan O D and Diamond P H 2015 *Phys. Plasmas* **22** 090702

[30] Li B, Sun C K, Wang X Y, Zhou A, Wang X G and Ernst D R 2015 *Phys. Plasmas* **22** 112304

[31] Yu C, Brower D L, Zhao S, Bravenec R V, Chen J, Lin H, Luhmann Jr N C, Peebles W A, Ritz C P, Schoch P M and Yang X 1992 *Nucl. Fusion* **32** 1545

[32] McDevitt C J and Diamond P H 2006 *Phys. Plasmas* **13** 032302

[33] Itoh S I, Itoh K and Yagi M 2003 *Phys. Rev. Lett.* **91** 045003

[34] Yagi M, Itoh S I, Itoh K, Azumi M, Diamond P H, Fukuyama A and Hayashi T 2007 *Plasma Fusion Res.* **2** 25

[35] Militello F, Waelbroeck F L, Fitzpatrick R and Horton W 2008 *Phys. Plasmas* **15** 050701

[36] Sen A, Singh R, Chandra D, Kaw P and Raju D 2009 *Nucl. Fusion* **49** 115012

[37] Poli E, Bottino A, Hornsby W A, Peeters A G, Ribeiro T, Scott B D and Siccinio M 2010 *Plasma Phys. Control. Fusion* **52** 124021

[38] Muraglia M, Agullo O, Benkadda S, Yagi M, Garbet X and Sen A 2011 *Phys. Rev. Lett.* **107** 095003

[39] Zhao K J, Shi Y J, Hahn S H, Diamond P H, Sun Y, Cheng J, Liu H, Lie N, Chen Z P, Ding Y H, Chen Z Y, Rao B, Leconte M, Bak J G, Cheng Z F, Gao L, Zhang X Q, Yang Z J, Wang N C, Wang L, Jin W, Yan L W, Dong J Q, Zhuang G and J-TEXT team 2015 *Nucl. Fusion* **55** 073022

[40] Zarzoso D, Hornsby W A, Poli E, Casson F J, Peeters A G and Nasr S 2015 *Nucl. Fusion* **55** 113018

[41] Hill P, Hariri F and Ottaviani M 2015 *Phys. Plasmas* **22** 042308

[42] Hornsby W A, Migliano P, Buchholz R, Kroenert L, Weikl A, Peeters A G, Zarzoso D, Poli E and Casson F J 2015 *Phys. Plasmas* **22** 022118

[43] Bardóczi L, Rhodes T L, Carter T A, Bañón Navarro A, Peebles W A, Jenko F and McKee G 2016 *Phys. Rev. Lett.* **116** 215001

[44] Navarro A B, Bardóczi L, Carter T A, Jenko F and Rhodes T L 2017 *Plasma Phys. Control. Fusion* **59** 034004

[45] Chen W, Jiang M, Xu Y, Shi P W, Yu L M, Ding X T, Shi Z B, Ji X Q, Yu D L, Li Y G, Yang Z C, Zhong W L, Qiu Z Y, Li J Q, Dong J Q, Yang Q W, Liu Y, Yan L W, Xu M and Duan X R 2017 *Nucl. Fusion* **57** 114003

[46] Jiang M, Zhong W L, Xu Y, Shi Z B, Chen W, Ji X Q, Ding X T, Yang Z C, Shi P W, Liang A S, Wen J, Li J Q, Zhou Y, Li Y G, Yu D L, Liu Y, Yang Q W and HL-2A Team 2018 *Nucl. Fusion* **58** 026002

[47] Wang Z X, Li J Q, Kishimoto Y and Dong J Q 2009 *Phys. Plasmas* **16** 060703

[48] Ishizawa A and Diamond P H 2010 *Phys. Plasmas* **17** 074503

[49] Jiang P, Lin Z, Holod I and Xiao C 2014 *Phys. Plasmas* **21** 122513

[50] Hu S, Li J, Qu H and Kishimoto Y 2014 *Phys. Plasmas* **21** 102508

[51] Izacard O, Holl, C, James S D and Brennan D P 2016 *Phys. Plasmas* **23** 022304

[52] Wang Z X, Li J Q, Dong J Q and Kishimoto Y 2009 *Phys. Rev. Lett.* **103** 015004

[53] Wilson H R and Connor J W 2009 *Plasma Phys. Control. Fusion* **51** 115007

[54] Waelbroeck F L, Militellol F, Fitzpatrick R and Horton W 2009 *Plasma Phys. Control. Fusion* **51** 015015

[55] Li J, Kishimoto Y, Kouduki Y, Wang Z X and Janvier M 2009 *Nucl. Fusion* **49** 095007

[56] Li J and Kishimoto Y 2012 *Phys. Plasmas* **19** 030705

[57] Hornsby W A, Peeters A G, Snodin A P, Casson F J, Camenen Y, Szepesi G, Siccinio M and Poli E 2010 *Phys. Plasmas* **17** 092301

[58] Ishizawa A and Nakajima N 2007 *Nucl. Fusion* **47** 1540

[59] Agullo O, Muraglia M, Poyé A, Benkadda S, Yagi M, Garbet X and Sen A 2014 *Phys. Plasmas* **21** 092303

[60] Hammett G W and Perkins F W 1990 *Phys. Rev. Lett.* **64** 3019

[61] Snyder P B and Hammett G W 2001 *Phys. Plasmas* **8** 3199

[62] Hamaguchi S and Horton W 1990 *Phys. Fluids B* **2** 1833

[63] Horton W and Estes R D 1980 *Plasma Phys.* **22** 663

[64] Gao Z, Dong J Q, Liu G J and Ying C T 2002 *Phys. Plasmas* **9** 1692

[65] Hahm T S and Tang W M 1989 *Phys. Fluids B* **1** 1185

[66] Wei L, Wang Z X, Hu Z Q, Li J Q and Kishimoto Y 2015 *Phys. Plasmas* **22** 112505

[67] Mattor N and Parker S 1997 *Phys. Rev. Lett.* **79** 3419

[68] Weil J, Liu C S and Zagorodny A 2015 *J. Plasma Phys.* **81** 905810101

[69] Kishimoto Y, Kim J Y, Horton W, Tajima T, LeBrun M J and Shirai H 1999 *Plasma Phys. Control. Fusion* **41** A663

[70] Miki K, Kishimoto Y, Miyato N and Li J Q 2007 *Phys. Rev. Lett.* **99** 145003

[71] Xie H S, Xiao Y and Lin Z 2017 *Phys. Rev. Lett.* **118** 095001

[72] Han M K, Wang Z X, Dong J Q and Du H 2017 *Nucl. Fusion* **57** 046019

[73] Ishizawa A, Waelbroeck F L, Fitzpatrick R, Horton W and Nakajima N 2012 *Phys. Plasmas* **19** 072312

[74] Hu Z Q, Wang Z X, Wei L, Li J Q and Kishimoto Y 2014 *Nucl. Fusion* **54** 123018

[75] Sun P J, Li Y D, Ren Y, Zhang X D, Wu G J, Lyu B, Shi T H, Xu L Q, Wang F D, Li Q, Zhang J Z, Hu L Q, Li J G and EAST team 2018 *Plasma Phys. Control. Fusion* **60** 025019